



1

## 1 A High-Resolution Air-Sea Synoptic Observation

## 2 Dataset from Drifting Buoys in the Bay of Bengal

3 Wei Huang<sup>1</sup>, Guihua Wang<sup>1,2</sup>, Changlin Chen<sup>1,2</sup>, Gengxin Chen<sup>3</sup>, Weiqiang Wang<sup>3</sup>

4 <sup>1</sup>*Department of Atmospheric and Oceanic Sciences & Institute of Atmospheric Sciences, Fudan*  
5 *University, Shanghai, 200438, China*

6 <sup>2</sup>*Shanghai Key Laboratory of Ocean-land-atmosphere Boundary Dynamics and Climate Change,*  
7 *Shanghai, 200438, China*

8 <sup>3</sup>*South China Sea Institute of Oceanology, Chinese Academy of Sciences, Guangzhou, 510301, China*

9 Correspondence to: Guihua Wang (wanggh@fudan.edu.cn)

10 **Abstract.** Mass and heat exchanges at the air-sea interface fundamentally drive global weather and  
11 climate systems. However, acquiring long-term, high-frequency, synchronous in-situ observations of  
12 both atmosphere and oceanic variables remains highly challenging, especially during extreme weather.  
13 This paper presents a high-resolution dataset from five air-sea drifting buoys deployed in the Bay of  
14 Bengal (BoB) in 2020 and 2022. These buoys captured precise, synchronous measurements of key  
15 meteorological parameters (air temperature, sea-level pressure, wind speed and direction, and relative  
16 humidity) alongside sea surface temperature. The dataset is typically sampled hourly; however, the  
17 sampling was increased to 5-minute intervals during tropical cyclones Nivar, Burevi, Four and Asani.  
18 This high-frequency dataset offers invaluable in-situ records for studying diurnal variations and fine-  
19 scale processes in the BoB. Furthermore, it provides critical observational data to advance our  
20 understanding of air-sea coupling, validate high-frequency satellite products, and improve  
21 parameterizations in regional numerical weather prediction models under extreme conditions.

### 22 23 1 Introduction

24 The air-sea interface is a critical boundary for mass, heat, and momentum exchange, directly driving  
25 the global climate and regional weather systems (Cronin et al., 2019). However, acquiring long-term,  
26 high-frequency, synchronous in-situ observations of both atmospheric and oceanic variables remains a  
27 major challenge (Bourassa et al., 2013). Widely deployed drifting buoy arrays (e.g., SVP buoys in the  
28 Global Drifter Program) offer extensive spatial coverage but typically measure only sea surface  
29 temperature (SST) and surface currents, lacking synchronous atmospheric observations (Lumpkin and  
30 Pazos, 2007; Centurioni, 2018). Conversely, moored buoys provide multi-variable time series but lack  
31 spatial mobility, limiting their ability to capture fast-moving meso- and submesoscale air-sea processes.  
32 Consequently, datasets from advanced air-sea drifting buoys capable of high-frequency, synchronous  
33 multi-variable observations remain exceedingly scarce.

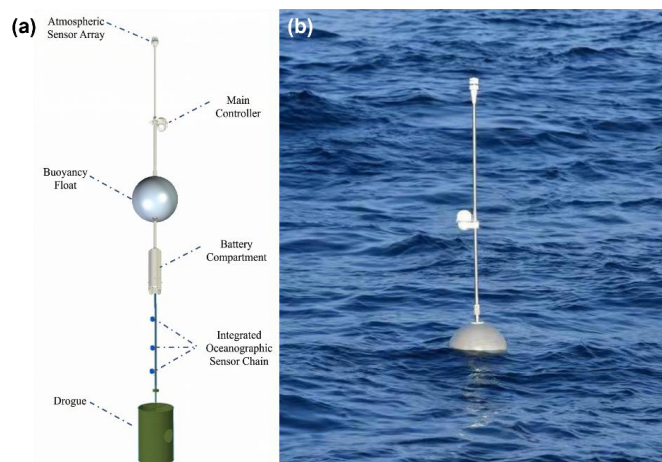
34 The Bay of Bengal (BoB) serves as an ideal natural laboratory for studying multi-scale air-sea  
35 interactions (Mahadevan et al., 2016). This region is heavily influenced by monsoons, driving complete  
36 reversals in surface circulation and intense eddy activity (Shankar et al., 2002). Furthermore, intense  
37 precipitation and substantial river runoff create a strong near-surface freshwater "barrier layer". This  
38 stratification suppresses the vertical mixing of cooler subsurface waters, maintaining post-monsoon SSTs  
39 typically above 30°C (Weller et al., 2016). This profoundly modulates upper-ocean diurnal variations  
40 and creates a unique thermodynamic environment that not only fuels the genesis and rapid intensification  
41 of tropical cyclones (TCs) (Singh and Roxy, 2022), but also contributes to the high frequency of cyclonic



2

42 events in this basin (Bhardwaj and Singh, 2020).

43 Given the BoB's extreme dynamical complexity and frequent severe weather, high-resolution in-  
44 situ observations are essential. While existing moored networks (e.g., RAMA, McPhaden et al., 2009;  
45 OMNI, Venkatesan et al., 2013) provide essential baseline climatological data, they face severe  
46 survivability challenges during TC-induced extreme sea states. To address this gap, this study releases a  
47 dataset from five high-resolution air-sea drifting buoys deployed in the BoB in 2020 and 2022. A key  
48 strength of this dataset is its dual capacity for long-term baseline monitoring and high-frequency extreme  
49 event capture. Under typical conditions, the buoys recorded stable hourly measurements; during severe  
50 TCs (Nivar, Burevi, Four and Asani), sampling frequency increased to 5–30 minute intervals. Spanning  
51 typical diurnal cycles to extreme wind forcing, this ultra-high-resolution dataset is vital for uncovering  
52 fine-scale BoB ocean dynamics and serves as an irreplaceable benchmark for improving air-sea flux  
53 parameterizations in numerical weather prediction models under extreme conditions.



54  
55 **Figure 1. Overview of the drifting buoy system. (a) Structural diagram; (b) in-situ photograph of the buoy**  
56 **deployed at sea. The system consists of a main body, a sensor chain, and a drogue. Atmospheric sensors are**  
57 **mounted 2 m above the sea surface, with a satellite transceiver housed in the middle section for data**  
58 **transmission. The underwater sensor chain attaches to the bottom of the battery compartment, while the**  
59 **suspended drogue ensures Lagrangian (flow-following) capability.**

60

## 61 **2 Drifting buoys**

62 The drifting buoy system used in this dataset, developed by the Department of Atmospheric and  
63 Oceanic Sciences, Fudan University, integrates atmospheric and oceanic sensors (Figure 1). Utilizing the  
64 BeiDou Navigation Satellite System (BDS) for real-time positioning and data transmission, it provides  
65 continuous Lagrangian observations of key parameters: wind speed and direction, air temperature,  
66 relative humidity, sea-level pressure, and SST. The atmospheric module is mounted at a standard height  
67 above the sea surface, while the temperature sensor is positioned just below the waterline. To capture  
68 high-frequency air-sea interactions, the core sensors feature high precision (e.g., 0.1 hPa for air pressure,  
69 0.1 °C for air temperature and 0.001°C for SST). Table 1 summarizes the detailed technical specifications  
70 for all sensors. The system defaults to hourly sampling, which can be intensified to 5, 10, or 30 minutes  
71 via satellite command during extreme events like TCs.

72



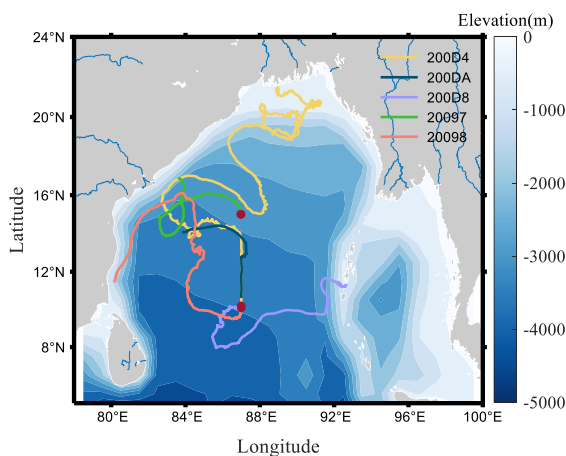
3

73 **Table 1. Specifications of the sensors equipped on the drifting air-sea interface buoys.**

Parameter	Sensor Type	Measurement Range	Accuracy	Resolution
Wind speed	AirMar 200WX-IPX7	0 to 40 m/s	±5% at 10m/s	0.1 m/s
Wind direction	AirMar 200WX-IPX7	0° to 359.9°	±3° at 10m/s	0.1°
Air temperature	AirMar 200WX-IPX7	-40°C to 80°C	±0.3°C at 20°C	0.1°C
Air pressure	AirMar 200WX-IPX7	300 to 1100 hPa	±0.5 hPa at 25°C	0.1 hPa
Relative humidity	VMS-3000- WS-N01	0% to 100%RH	±3% at 60%RH, 25°C	0.1%
Sea surface temperature	DW12	-5°C to 35°C	±0.01°C	0.001°C

74

75 The five buoys were deployed in the BoB in two batches (Figure 2). The first batch was deployed  
 76 in November 2020 at (87°E, 15°N) and (87°E, 9.8°N) for buoys 20097 and 20098, respectively. Drifting  
 77 through a mesoscale eddy and the southward-flowing western boundary current during autumn and  
 78 winter (Mukherjee et al., 2014), these buoys captured continuous observations during TCs Nivar and  
 79 Burevi. They averaged 68 operational days and yielded 12,355 valid records. The second batch was  
 80 deployed in April 2022 around 87°E, 10.1°N for the three buoys of 200D4, 200D8, and 200DA. Notably,  
 81 two of these buoys drifted in close parallel for an extended period, providing unique data on meso- and  
 82 submesoscale spatial correlations. This batch recorded the air-sea responses to TCs Asani and Four,  
 83 averaging 80 operational days (up to 150 days) and accumulating 127,199 valid records.



84

85 **Figure 2. Trajectories of the five drifting buoys in the BoB. Solid red dots indicate the initial deployment**  
 86 **positions, and background shading represents bathymetry. Colored lines denote the drift paths of individual**  
 87 **buoys: 200D4 (yellow), 200DA (black), 200D8 (purple), 20097 (green), and 20098 (red).**

88

89 **Table 2. List and information of drifting buoys.**



Device Name	Start time	End time	Synoptic Observations	Sample Frequencies	Sample Size	Tropical Cyclone
20097	2020/10/24	2021/01/01	Air: airt, windspd, winddir, apre, hum Ocean: sst Others : speed, attitude	5min, 10min, 1h	5306	Nivar, Burevi
20098	2020/10/27	2021/01/01	Air: airt, windspd, winddir, apre, hum Ocean: sst Others : speed, attitude	5min, 10min, 30min, 1h	7049	Nivar, Burevi
200D4	2022/04/17	2022/09/13	Air: airt, windspd, winddir, apre, hum Ocean: sst Others : speed, attitude	5min, 1h	115800	Tropical Cyclone Asani, Four
200D8	2022/04/17	2022/06/16	Air: airt, windspd, winddir, apre, hum Ocean: sst Others : speed, attitude	5min, 1h	9457	Tropical Cyclone Asani
200DA	2022/04/17	2022/05/15	Air: airt, windspd, winddir, apre, hum Ocean: sst Others : speed, attitude	5min, 10min	1942	Tropical Cyclone Asani

90

### 91 3 Data Processing Method

#### 92 3.1 Data Preprocessing and Quality Control

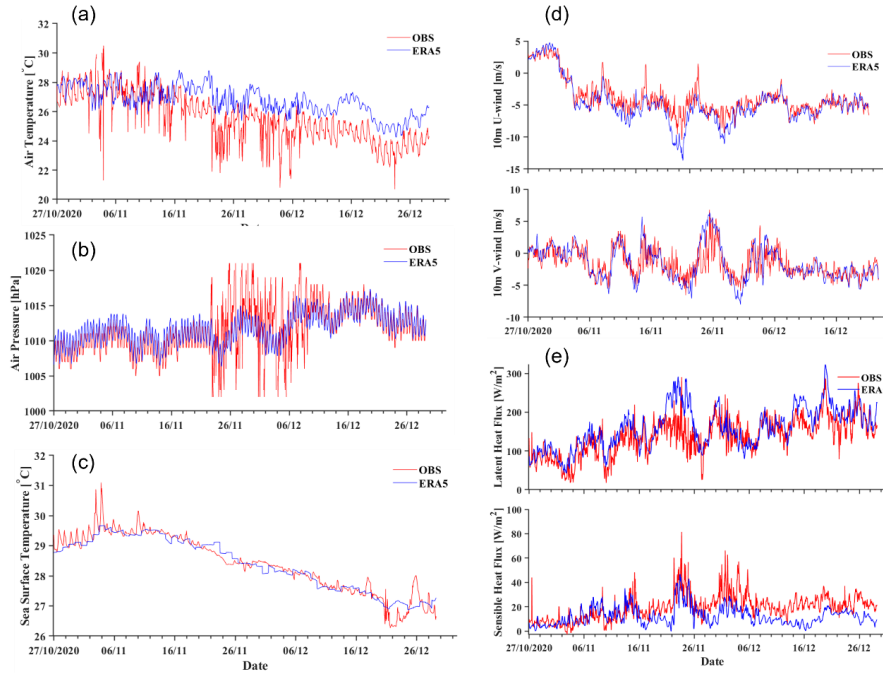
93 To ensure data reliability, all raw observations underwent a standardized quality control (QC)  
 94 workflow. First, the time series were uniformly standardized to Coordinated Universal Time (UTC) to  
 95 maintain temporal consistency. Second, a rigorous two-step QC procedure—comprising outlier removal  
 96 and ERA5 reanalysis validation—was applied to address sensor noise and environmental unpredictability.

97 **Outlier Removal:** Raw data inevitably contain anomalous spikes. We employed a two-step  
 98 cleaning method. First, a physical range check removed values exceeding climatological norms or  
 99 instrument limits (e.g., unrealistic wind speed spikes). Next, we applied a three-sigma ( $3\sigma$ ) criterion to  
 100 filter any remaining anomalies: values deviating from the mean by more than three standard deviations  
 101 were flagged as outliers. All identified outliers were replaced with missing values (NaN), allowing users  
 102 to interpolate as needed.

103 **ERA5 Validation:** We compared our data against the ECMWF ERA5 reanalysis dataset (Hersbach  
 104 et al., 2020). Buoy measurements were temporally synchronized with ERA5's hourly data. Overall, the  
 105 buoy observations show high consistency with ERA5 in low-frequency trends. Specifically, sea-level  
 106 pressure (Figure 3b) and SST (Figure 3c) align closely, accurately reflecting synoptic weather passages  
 107 and thermal background evolution. However, for dynamically volatile parameters like zonal and  
 108 meridional wind components (Figure 3d) and air-sea heat fluxes (Figure 3e), the in-situ measurements  
 109 exhibit clear advantages. Constrained by spatial-smoothing and lower temporal resolution, ERA5 tends  
 110 to underestimate transient extremes during severe weather, such as TCs.



5



111

112 **Figure 3.** Time-series comparison of Buoy 20098 observations (red lines) and ERA5 reanalysis data (blue  
 113 lines). Buoy measurements were adjusted to a 10 m reference height and interpolated to hourly intervals for  
 114 synchronization. Panels show: (a) air temperature, (b) sea-level pressure, (c) SST, (d) u- and v-component  
 115 wind speeds, and (e) latent and sensible heat fluxes.

116

### 117 3.2 Current Velocity and Direction

118 Since surface ocean currents primarily drive the motions of the buoys, their high-precision  
 119 positioning and time-series data were used to derive surface velocity and direction. The surface current  
 120 was decomposed into a zonal component ( $u$ , positive eastward) and a meridional component ( $v$ , positive  
 121 northward), measured in m/s. The calculation formulas are as follows:

$$122 \quad u = \frac{(lon_1 - lon_0) \cdot \frac{\pi}{180} \cdot R \cdot \cos\left(\frac{lat_0 + lat_1}{2} \cdot \frac{\pi}{180}\right)}{t_1 - t_0}$$

$$123 \quad v = \frac{(lat_1 - lat_0) \cdot \frac{\pi}{180} \cdot R}{t_1 - t_0}$$

124 where  $lon_2$ ,  $lon_1$  and  $lat_2$ ,  $lat_1$  are the longitudes and latitudes (in degrees) at adjacent observation  
 125 times  $t_2$  and  $t_1$ ; and  $R$  is the mean radius of the Earth (6371 km).

### 126 3.3 Air-Sea Heat Fluxes

127 Air-sea interactions are fundamentally governed by interfacial momentum and heat exchanges. The  
 128 multi-variable buoy observations (air temperature, SST, relative humidity, and wind speed) provide  
 129 essential in-situ data for estimating these fluxes (Zhang et al., 2024). We employed the Coupled Ocean-  
 130 Atmosphere Response Experiment (COARE) bulk parameterization algorithm (version 3.0) to calculate



6

131 sensible heat (SH) and latent heat (LH) fluxes (Fairall et al., 2003).

132 The core equations are as follows:

$$133 \quad SH = \rho C_{p_a} C_H U (SST - T_a)$$

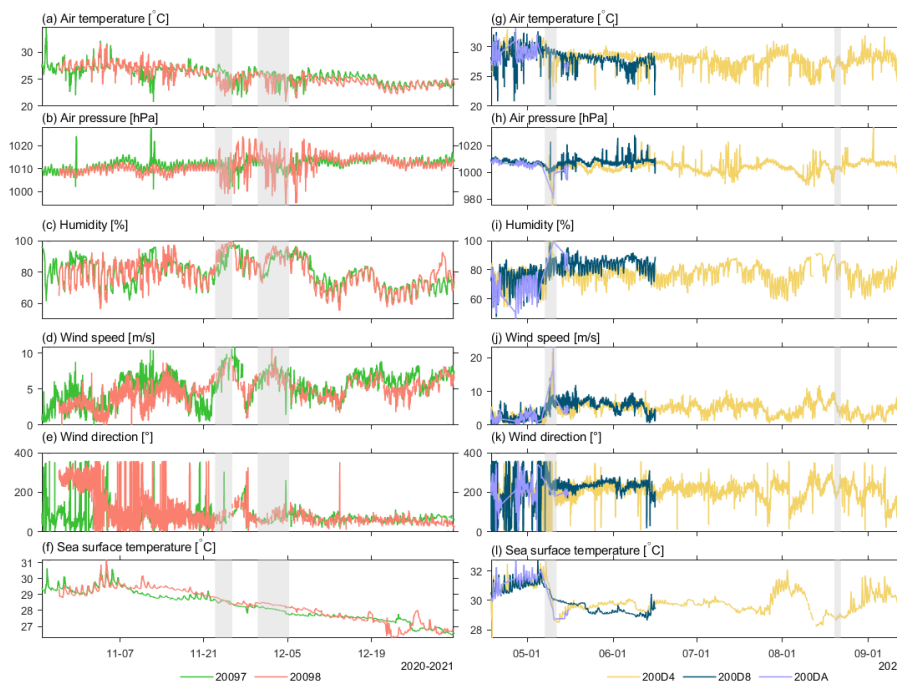
$$134 \quad LH = \rho L_e C_E U (q_s - q_a)$$

135 where  $\rho$  is the density of air;  $C_{p_a}$  is the specific heat capacity of air at constant pressure;  $L_e$  is the latent  
 136 heat of vaporization of water;  $U$  is the near-surface wind speed; SST is the surface temperature;  $T_a$   
 137 is the air temperature;  $q_s$  and  $q_a$  are the specific humidities at the sea surface and in the near-surface air,  
 138 respectively;  $C_H$  and  $C_E$  are the sensible and latent heat transfer coefficients. Since COARE 3.0  
 139 requires inputs standardized to specific heights, we adjusted our 2.0 m meteorological observations to  
 140 the standard 10 m reference height using empirical profile formulas prior to calculation.

141

#### 142 4 Data overview

143 Figure 2 illustrates the complete trajectories of the five drifting buoys in the BoB. Despite initial  
 144 deployments near the 87°E transect, their drift paths diverged significantly, encountering multiple  
 145 extreme weather events, including TCs (Table 2), and recording highly variable air-sea conditions.  
 146 Driven by cyclonic circulation, the winter 2020 buoys (20097, 20098) followed complex spiral  
 147 trajectories in the central BoB, capturing mesoscale eddies, the southward-flowing western boundary  
 148 current, and TCs Nivar and Burevi. Conversely, the summer 2022 buoys (200D4, 200D8, 200DA)  
 149 exhibited more coherent trajectories across a broader area, recording the passages of Tropical Cyclone  
 150 Asani and Four. Together, these datasets provide essential in-situ support for investigating monsoon  
 151 transitions and air-sea interactions in the BoB.



152

153 **Figure 4.** Time series of observed meteorological and oceanic parameters. Left-column panels show data for  
 154 buoys 20097 (green) and 20098 (red); right-column panels show buoys 200D4 (yellow), 200D8 (blue), and



7

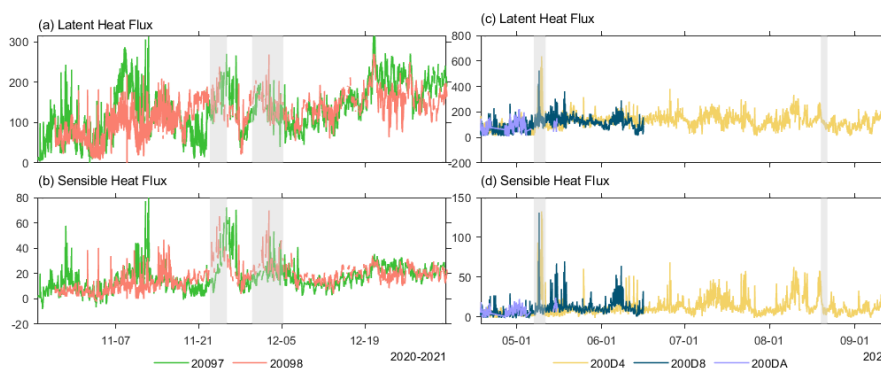
155 **200DA (purple). Gray-shaded areas indicate TC passages: Nivar and Burevi (left), and Cyclonic Storm Asani**  
156 **and Tropical Depression Four (right). Panels show: (a, g) air temperature, (b, h) sea-level pressure, (c, i)**  
157 **relative humidity, (d, j) wind speed, (e, k) wind direction, and (f, l) SST.**

158

159 The buoys continuously recorded key meteorological parameters, including air temperature, sea-  
160 level pressure, relative humidity, wind speed, and SST (Figure 4). Under typical conditions, air  
161 temperature (21–35 °C) and SST exhibited clear diurnal cycles, with SST generally exceeding air  
162 temperature. While the high-frequency amplitude of SST was smaller, it displayed distinct seasonal  
163 warming and cooling trends. Wind speeds typically ranged from 0 to 10 m/s under normal conditions but  
164 sharply increased during TC encounters. For example, during TC Asani, wind speeds exceeded 20 m/s,  
165 driving dramatic environmental changes at the air-sea interface. Sea-level pressure exhibited a signature  
166 plunge (Figures 4b, 4h), accompanied by abrupt responses in SST, air temperature, and relative humidity.

167 Notably, extreme wind forcing from TCs triggered a surge in air-sea heat fluxes (Figure 5). The  
168 instantaneous peak of LH flux reached 636.6 W/m<sup>2</sup>, far exceeding normal baseline levels. These high-  
169 frequency records provide robust in-situ evidence for quantifying momentum and heat exchanges under  
170 extreme TC forcing.

171 In summary, this high-resolution dataset integrates atmospheric and oceanic variables, heat fluxes,  
172 and surface current data. By capturing continuous observations across diverse spatiotemporal scales and  
173 extreme weather conditions, it offers essential empirical support for analyzing meso- and submesoscale  
174 processes, ocean fronts, fine-scale air-sea interactions, and monsoon dynamics, while also aiding the  
175 improvement of extreme weather forecasting models.



176

177 **Figure 5. Time series of air-sea heat fluxes. Left-column panels show data for buoys 20097 (green) and 20098**  
178 **(red); right-column panels show buoys 200D4 (yellow), 200D8 (blue), and 200DA (purple). Gray-shaded areas**  
179 **indicate TC passages: Nivar and Burevi (left), and Cyclonic Storm Asani and Tropical Depression Four**  
180 **(right). Panels show: (a, c) latent heat flux (LH), and (b, d) sensible heat flux (SH).**

181

## 182 5 Data availability

183 The high-resolution air-sea interface drifting buoy dataset in the Bay of Bengal described in this  
184 study is publicly available in the Zenodo repository and can be freely accessed via the following DOI:  
185 <https://doi.org/10.5281/zenodo.19469106> (Huang et al., 2026).

186

## 187 6 Discussion and conclusion



188 This study presents a high-frequency observational dataset from five air-sea drifting buoys deployed  
189 in the BoB during the winter 2020 and summer 2022 cruises. Rigorous quality control effectively  
190 removed anomalous noise from the raw observations. Comparisons with the ERA5 reanalysis not only  
191 confirm the dataset's overall reliability but also demonstrate its capability to capture fine-scale transient  
192 signals during extreme sea states. Beyond fundamental meteorological variables, this standardized  
193 product includes derived surface ocean current velocities and COARE 3.0-estimated air-sea heat fluxes,  
194 offering substantial scientific value.

195 Characterized by high-frequency, synchronous multi-variable observations, this dataset holds  
196 significant potential for multi-scale oceanographic and meteorological research. These records provide  
197 scarce in-situ data for investigating fine-scale boundary layer dynamics and rapid air-sea flux responses.  
198 Notably, the data captured during TCs offer vital empirical evidence for understanding strong air-sea  
199 coupling mechanisms under extreme forcing. Furthermore, these continuous, high-precision  
200 observations can validate high-frequency satellite products (e.g., microwave radiometers and  
201 scatterometers), evaluate reanalysis datasets, and optimize flux parameterizations in regional numerical  
202 models.

203 While rigorous quality control was applied, we acknowledge the inherent limitations of Lagrangian  
204 platforms (Centurioni et al., 2019). First, wind- and current-driven drift trajectories preclude long-term  
205 Eulerian time-series analysis at fixed locations. Second, extreme sea states with severe wave breaking  
206 and sea spray may occasionally introduce transient noise into the measurements. Nevertheless, our  
207 systematic processing workflow effectively identifies and mitigates these anomalies, maximizing the  
208 rigor and reliability of this published dataset.

209

#### 210 **Acknowledgements.**

211 This work was supported by the National Natural Science Foundation of China (NSFC, 42288101),  
212 the Science and Technology Commission of Shanghai Municipality (25DZ3102200), and the Guidance  
213 Project for Industrial Technology Development and Application Plan of Fujian Province (2024Y0075).  
214 The first batch was deployed by the open research cruise NORC2020-10, supported by the NSFC  
215 Shiptime Sharing Project (41949910), and the second batch was deployed by the open research cruise  
216 NORC2022-10, supported by the NSFC Shiptime Sharing Project (42149910). Both deployment cruises  
217 were implemented by the SCSIO R/V “SHIYAN 6”.

218

#### 219 **Appendix A: Additional tables**

220

221 **Table A1 Tropical cyclone information.**

Tropical Cyclone Name	Year	Start Time	End Time
Niviar	2020	2020.11.22 21	2020.11.25 18
Burevi	2020	2020.11.30 00	2020.12.05 06
Asani	2022	2022.05.07 06	2022.05.11 12
Four	2022	2022.08.19 15	2022.08.22 00

222 TC information comes from website of India Meteorological Department  
223 ([https://rsmcnnewdelhi.imd.gov.in/report.php?internal\\_menu=MzM=](https://rsmcnnewdelhi.imd.gov.in/report.php?internal_menu=MzM=))

224



225 **References**

- 226 Bhardwaj, P. and Singh, O.: Climatological characteristics of Bay of Bengal tropical cyclones: 1972–  
227 2017, *Theoretical and Applied Climatology*, 139, 615-629, <https://doi.org/10.1007/s00704-019-02989-4>,  
228 2020.
- 229 Bourassa, M. A., Gille, S. T., Bitz, C., Carlson, D., Cerovecki, I., Clayson, C. A., Cronin, M. F., Drennan,  
230 W. M., Fairall, C. W., Hoffman, R. N., Magnusdottir, G., Pinker, R. T., Renfrew, I. A., Serreze, M.,  
231 Speer, K., Talley, L. D., and Wick, G. A.: High-latitude ocean and sea ice surface fluxes: Challenges and  
232 opportunities, *Bulletin of the American Meteorological Society*, 94(3), 403-430,  
233 <https://doi.org/10.1175/BAMS-D-11-00244.1>, 2013.
- 234 Centurioni, L. R.: Drifter technology and impacts for sea surface temperature, sea-level pressure, and  
235 ocean circulation studies, in: *Observing the Oceans in Real Time*, edited by: Venkatesan, R., Tandon, A.,  
236 D'Asaro, E., and Atmanand, M. A., Springer, Cham, 37-57, [https://doi.org/10.1007/978-3-319-66493-4\\_3](https://doi.org/10.1007/978-3-319-66493-4_3), 2018.
- 238 Centurioni, L. R., Turton, J., Lumpkin, R., Braasch, L., Brassington, G., Chao, Y., Charpentier, E., Chen,  
239 Z., Corlett, G., and others: Global in situ observations of essential climate and ocean variables at the air–  
240 sea interface, *Frontiers in Marine Science*, 6, 419, <https://doi.org/10.3389/fmars.2019.00419>, 2019.
- 241 Cronin, M. F., Gentemann, C. L., Edson, J., Ueki, I., Bourassa, M., Brown, S., Clayson, C. A., Fairall,  
242 C. W., Farrar, J. T., Gille, S. T., Gulev, S., Josey, S. A., Kato, S., Katsumata, M., Kent, E., Roemmich,  
243 D., Weller, R. A., Wick, G. A., Williams, I., and Yu, L.: Air-sea fluxes with a focus on heat and  
244 momentum, *Frontiers in Marine Science*, 6, 430, <https://doi.org/10.3389/fmars.2019.00430>, 2019.
- 245 Fairall, C. W., Bradley, E. F., Hare, J. E., Grachev, A. A., and Edson, J. B.: Bulk parameterization of air–  
246 sea fluxes: Updates and verification for the COARE algorithm, *Journal of Climate*, 16(4), 571-591,  
247 [https://doi.org/10.1175/1520-0442\(2003\)016<0571:BPOASF>2.0.CO;2](https://doi.org/10.1175/1520-0442(2003)016<0571:BPOASF>2.0.CO;2), 2003.
- 248 Hersbach, H., Bell, B., Berrisford, P., Hirahara, S., Horányi, A., Muñoz-Sabater, J., Nicolas, J., Peubey,  
249 C., Radu, R., Schepers, D., Simmons, A., Soci, C., and others: The ERA5 global reanalysis, *Quarterly*  
250 *Journal of the Royal Meteorological Society*, 146(730), 1999-2049, <https://doi.org/10.1002/qj.3803>,  
251 2020.
- 252 Huang, W., Wang, G., Chen, C., Chen, G., and Wang, W.: A High-resolution Air-Sea Synoptic  
253 Observation Dataset from Drifting Buoys in the Bay of Bengal, Zenodo [dataset],  
254 <https://doi.org/10.5281/zenodo.19469106>, 2026.
- 255 Lumpkin, R. and Pazos, M.: Measuring surface currents with Surface Velocity Program drifters: the  
256 instrument, its data, and some recent results, in: *Lagrangian Analysis and Prediction of Coastal and*  
257 *Ocean Dynamics*, edited by: Griffa, A., Kirwan, A. D., Mariano, A. J., Özgökmen, T., and Rossby, T.,  
258 Cambridge University Press, 39-67, <https://doi.org/10.1017/CBO9780511535901.003>, 2007.
- 259 Mahadevan, A., Paluszkiwicz, T., Ravichandran, M., Sengupta, D., and Tandon, A.: Bay of Bengal:  
260 From monsoons to mixing, *Oceanography*, 29(2), 14-17, <https://doi.org/10.5670/oceanog.2016.34>, 2016.
- 261 McPhaden, M. J., Meyers, G., Ando, K., Masumoto, Y., Murty, V. S. N., Ravichandran, M., Syamsudin,  
262 F., Vialard, J., Yu, L., and Qiu, W.: RAMA: The Research Moored Array for African–Asian–Australian  
263 Monsoon Analysis and Prediction, *Bulletin of the American Meteorological Society*, 90(4), 459-480,  
264 <https://doi.org/10.1175/2008BAMS2608.1>, 2009.
- 265 Mukherjee, A., Shankar, D., Fernando, V., Amol, P., Aparna, S. G., Fernandes, R., Michael, G. S.,  
266 Khalap, S. T., Satelkar, N. P., Agarvadekar, Y., Gaonkar, M. G., Tari, A. P., Kankonkar, A., and Vernekar,  
267 S.: Observed seasonal and intraseasonal variability of the East India Coastal Current on the continental  
268 slope, *Journal of Earth System Science*, 123(6), 1197-1232, <https://doi.org/10.1007/s12040-014-0471-7>,



10

- 269 2014.
- 270 Shankar, D., Vinayachandran, P. N., and Unnikrishnan, A. S.: The monsoon currents in the north Indian  
271 Ocean, *Progress in Oceanography*, 52(1), 63-120, [https://doi.org/10.1016/S0079-6611\(02\)00024-1](https://doi.org/10.1016/S0079-6611(02)00024-1), 2002.
- 272 Singh, V. K. and Roxy, M. K.: A review of ocean-atmosphere interactions during tropical cyclones in  
273 the north Indian Ocean, *Earth-Science Reviews*, 226, 103967,  
274 <https://doi.org/10.1016/j.earscirev.2022.103967>, 2022.
- 275 Venkatesan, R., Shamji, V. R., Latha, G., Mathew, S., Rao, R. R., Sengupta, D., and Arul Muthiah, M.  
276 A.: In situ ocean subsurface time-series measurements from OMNI buoy network in the Bay of Bengal,  
277 *Current Science*, 104(9), 1166-1177, 2013.
- 278 Weller, R. A., Farrar, J. T., Buckley, J., Mathew, S., Venkatesan, R., Sreejith, J., Surya Prakash, M., and  
279 Suresh Kumar, N.: Air-sea interaction in the Bay of Bengal, *Oceanography*, 29(2), 28-37,  
280 <https://doi.org/10.5670/oceanog.2016.36>, 2016.
- 281 Zhang, Y., Wang, B., Chen, Z., Song, X., Dang, C., Sun, D., Li, Y., Ma, X., and Wu, L.: Drifting Air-  
282 Sea Interface Buoy (DrIB): A Practical Platform for Global Air-Sea Observations, *Journal of*  
283 *Atmospheric and Oceanic Technology*, 42(11), 1457-1468, <https://doi.org/10.1175/JTECH-D-24-0080.1>,  
284 2024.